Journal of Fluids and Structures 76 (2018) 367–383

Contents lists available at ScienceDirect

Journal of Fluids and Structures

journal homepage: www.elsevier.com/locate/jfs

Flow-induced vibration of three unevenly spaced in-line cylinders in cross-flow

Mahmoud Shaaban, Atef Mohany *

Faculty of Engineering and Applied Science, University of Ontario Institute of Technology, Oshawa, ON, Canada

ARTICLE INFO

Article history:
Received 4 April 2017
Received in revised form 1 September 2017
Accepted 12 October 2017
Available online 15 November 2017

Keywords:
Cross-flow
Flow-induced vibration
Fluid forces
Tandem cylinders
Uneven spacing
Vortex shedding
Energy harvesting

ABSTRACT

The flow over three cylinders arranged in-line with uneven spacing in cross-flow is numerically investigated at a Reynolds number of 200. The center-to-center distance between the upstream and the most downstream cylinder was kept constant at 4 diameters. The distance between the inline centers of the upstream and middle cylinders (x) was studied in the range of 1.05 to 2.95 diameters. The flow structure around the cylinders shows two distinctive patterns of vortex shedding, one of which occurs at $x = 1.60$ and 1.80 diameters, and causes significantly higher oscillating lift and mean drag forces with a lower value of Strouhal number. At these middle cylinder locations, the shear layer reattaches on the downstream cylinder and results in vortex formation in the gap between the middle and downstream cylinders. On the other hand, at all other locations of the middle cylinder the shear layer does not reattach on the downstream cylinder. Moreover, when the middle cylinder is located at $x = 1.60$ or 1.80 diameters, the vortex formation length is shorter and the vorticity in the downstream vortex street is higher than the case when the middle cylinder is located at all other locations. To understand the effect of these distinctive flow features on the flow-induced vibration response of the most downstream cylinder, the coupling between the flow field and the cylinder motion is numerically modeled. As the reduced velocity is increased, the oscillation amplitude of the downstream cylinder increases to its maximum at lock-in, then it starts to decrease similar to the case of a single cylinder. However, the oscillation amplitude reaches a higher value than that observed for the case of vortex-induced vibration of both a single cylinder and two tandem cylinders. Moreover, significant oscillation amplitude is pertained at high reduced velocities with dependency on the uneven spacing between the cylinders. The frequency of oscillations increases at different rates in three different ranges of reduced velocities, indicating different energy transfer mechanisms. Although the frequency of vibration is shifted away from the structure resonance frequency at high reduced velocities, the significant amplitude of oscillations is attributed to the interaction of two opposing mechanisms that occur when the cylinder is at different positions in the cycle. The wide range of reduced velocities at which the cylinder vibrates with a significant amplitude makes the configuration of three in-line cylinders a good candidate for flow energy harvesting.

© 2017 Elsevier Ltd. All rights reserved.

1. Introduction

A group of cylinders in cross-flow is an arrangement that recurs abundantly in many engineering applications. Structures of cylindrical cross sections can be found in buildings, heat exchangers in power plants, silos, underwater pipelines,

* Corresponding author.
E-mail address: atef.mohany@uoit.ca (A. Mohany).

https://doi.org/10.1016/j.jfluidstructs.2017.10.007
0889-9746/© 2017 Elsevier Ltd. All rights reserved.

suspension and power cables, and many other applications in air, water, and multiphase flows. In some cases, the cylindrical structures are unevenly spaced, which is a distinct flow geometry that gives rise to flow patterns that are not thoroughly investigated. Fluid forces exerted on such configurations can cause failure or fretting wear, and therefore must be included in the design and operation considerations. For example, forces due to wind flow on structures such as tanks and silos can cause significant deflections and buckling (e.g. Portela and Godoy, 2005; Sosa and Godoy, 2005). Shedding of vortices around one or a group of cylinder-like structures can give rise to excessive noise (Mohany, 2006; Arafa and Mohany, 2015). In addition, flexible structures subject to flow are prone to vortex-induced vibration. Applications such as riser pipes in offshore oil fields, suspension cables in wind flow, highway light poles, data cables in underwater currents, and other applications can undergo vibrations of significant amplitudes which may endanger their operation (Weaver et al., 2000; Mohany et al., 2012; Hassan and Mohany, 2013).

An extensive review by Zdravkovich (1977) of the flow interference between two cylinders show that the flow field around a group of cylinders in close proximity subjected to cross-flow differs significantly from the case of isolated cylinders. Igarashi and Suzuki (1984) experimentally studied the characteristics of flow around three cylinders of equal diameters arranged inline with *even spacing*. They provided a detailed description of the flow patterns and fluid forces that occur in this arrangement, and reported bistable switching between the flow patterns. They described a complex combination of flow patterns around the cylinders. The observed patterns depend on the spacing between the cylinders and Reynolds number. However, it is unclear how the flow structure and the fluid forces acting on the cylinders would be affected if spacing between them was uneven. Zhang and Zhou (2001) investigated the effect of unequal cylinder spacing on the vortex streets behind three rigid side-by-side cylinders. They reported that slight inequalities in the spacing between the cylinders can lead to substantial changes in pressure distribution on cylinder surfaces, and therefore change lift and drag forces.

The safety concerns in many applications that include flexible structures in fluid flow sparked remarkable research efforts to understand the phenomenon of flow-induced vibration. Significant attention has been focused towards the cases of a single and two cylinders. Anagnostopoulos and Bearman (1992) conducted an experimental investigation of the vortex-induced vibration of a single cylinder in a fully laminar regime at a Reynolds number up to 150 and at a high mass ratio m^* of 149, as defined in Eq. (6). They observed that the maximum oscillation amplitude of 0.6 diameters occurs near the lower limit of the lock-in region. Khalak and Williamson (1997) investigated the occurrence of vortex-induced vibration of a cylinder free to vibrate in one direction at low mass ratio and structural damping of $m^* = 2.4$ and $\zeta = 0.0059$, respectively. They observed significantly higher amplitudes of oscillation compared to previous studies at higher solid to displaced fluid mass ratio. Govardhan and Williamson (2006) investigated the effect of Reynolds number on the amplitude of oscillations of a single cylinder for a fixed mass ratio of m^*=10. They observed a constant maximum oscillation amplitude of 0.6 diameters in laminar flows. However, they reported that the maximum oscillation amplitude depends on log (Re) in turbulent flows. Hover and Triantafyllou (2001) experimentally investigated the flow-induced vibration of two tandem cylinders with only the downstream cylinder allowed to vibrate at $m^* = 3.0$ and $\zeta = 0.04$. They reported a wider lock-in range and a higher amplitude of oscillation than that of a single cylinder. More interestingly, they reported significantly higher amplitudes of oscillation at higher reduced velocities. Assi et al. (2010) experimentally investigated the mechanism of flow-induced vibrations for two tandem cylinders when the downstream cylinder is allowed to vibrate. They observed that the oscillations are characterized by a build-up of amplitude persisting to high reduced velocities, which is different than the limited resonance range of vortex-induced vibration of a single cylinder. Although the vortex-induced vibration of two tandem cylinders has been thoroughly investigated, it is not clear whether this knowledge can be extended to multiple inline cylinders in cross-flow. The case of vortex-induced vibration from three or more inline cylinders in cross-flow has never been investigated. Furthermore, the problem becomes more complicated when the cylinders have uneven spacing between them and the vibration response cannot be directly inferred from the case of two tandem cylinders.

Recent development in numerical techniques and computational power allowed for accurate simulation of flow-induced vibration of many configurations. Meneghini et al. (2001) simulated the two-dimensional flow around two circular cylinders in tandem and side-by-side arrangements at Re = 200. They showed that spacing between the cylinders in both arrangements has a significant effect on the wake pattern and Strouhal number. Tandem cylinders at gaps lower than 3 diameters shed vortices only from the downstream cylinders. Harichandan and Roy (2010) simulated the two-dimensional incompressible flow around several configurations of cylinders of the same diameter at Re = 100 and 200. For flow past three cylinders in tandem, they observed that the downstream cylinder which lies in the wake of the upstream cylinder experiences very large unsteady forces that can give rise to vortex-induced vibrations. The wake of the two upstream cylinders is significantly different from the wake of a single cylinder and is influenced by the cylinder spacing and can give rise to bistable flow patterns. The effect of such wake features on the flow-induced vibration is not fully understood.

Mittal and Kumar (2001) numerically studied the flow-induced vibrations of a pair of cylinders in tandem and staggered arrangements in the wake interference flow regime at Re = 100 and $m^* = 4.72$. They observed that the forces on the upstream cylinder are similar to those observed for a single cylinder, whereas the downstream cylinder experiences significant unsteady forces. For systems where displaced fluid mass is relatively close to the solid mass, Mittal and Kumar (2001) suggested that vortex-shedding frequency of the oscillating cylinder at lock-in does not exactly match the structural resonance frequency. They also observed that the maximum oscillation amplitude of the spring–mass system does not change significantly even if the mass of the oscillator is reduced by a factor of 100. Borazjani and Sotiropoulos (2009) examined the accuracy of two-dimensional simulation by performing several three-dimensional simulations. Their results at Re = 100 and 200 show that three-dimensional instabilities are not sufficiently strong to alter the dynamic response

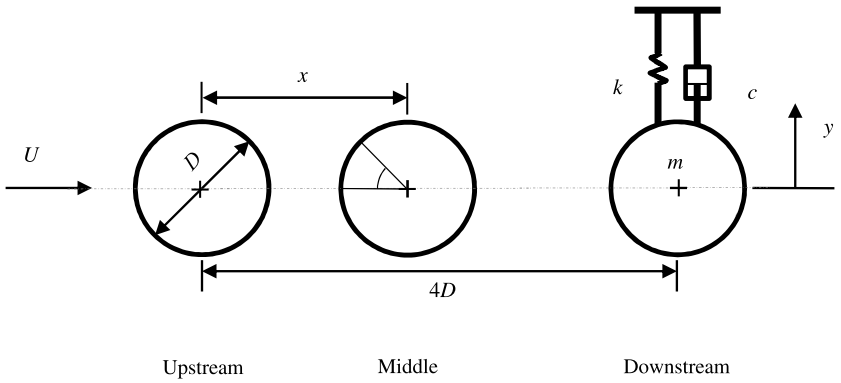


Fig. 1. A schematic of the studied model.

of the system, which for all simulated cases is found to be essentially identical to that observed for the two-dimensional system. Carmo et al. (2011) performed simulations of the vortex-induced vibration of two circular cylinders in tandem arrangement. In their simulations, the upstream cylinder was fixed and the downstream cylinder was free to oscillate in transverse direction. They simulated the flow at Re = 150 and low structural damping and mass ratio. They noted that the amplitude of oscillation for two tandem cylinders is higher than the case of a single cylinder and reported a notably higher amplitude of oscillation at higher reduced flow velocities. There is a need to extend the current knowledge to the flow-induced vibration in the case of three inline cylinders.

The vibration of flexible structures due to flow of wind or water currents can be used to develop innovative energy harvesting devices (e.g. Yoshitake et al., 2004; Barrero-Gil et al., 2012). Devices consisting of elastically-mounted cylindrical cables in cross-flow of wind or water currents can harvest energy at multiple natural frequencies of the structure (Bernitsas et al., 2008; Grouthier et al., 2014). Due to the significantly low energy densities in such applications and the varying operating conditions, it is favorable to have devices that can give higher response to a wider range of flow velocities. Therefore, there is a need to investigate the flow-induced vibration response of arrangements such as multiple in-line cylinders in cross-flow to assess their suitability as energy harvesting devices.

The situation of having unevenly spaced in-line cylinders in cross-flow is a challenging problem as it introduces another layer of complexity in terms of the flow-structure and the dynamic fluid forces acting on the cylinders that cannot be inferred from the simplified cases of a single cylinder or two cylinders in tandem. Such configuration has never been investigated before. For the case of three in-line cylinders in cross-flow, the most downstream cylinder is subjected to higher oscillating forces that are influenced by the upstream flow interactions. While an increase in the vibration amplitude is expected, the complex interaction between several parameters that influence the vibration response of the most downstream cylinder is rather ambiguous. Therefore, the main objective of this study is to investigate the flow structure around three unevenly-spaced in-line cylinders in cross-flow. In addition, the flow-induced vibration response of the downstream cylinder in such arrangements is investigated. The system with one degree of freedom would illustrate the first layer of information about the complex behavior of similar systems with higher degrees of freedoms, with more than one cylinder in the system allowed to move. The computational setup and the analysis procedure are discussed in the following section. After that, a discussion of the results is presented.

2. Governing equations and numerical model

The two-dimensional flow field around three unevenly-spaced inline rigid cylinders is simulated as described in this section. The gravity is not included in the formulation of body forces for neither the flow nor the structure domain. The reference length scale is the cylinder diameter D and the reference flow velocity is the upstream flow velocity U_∞. A schematic of the model is shown in Fig. 1. The simulations are performed at a Reynolds number of 200. The spacing between the axes of the upstream and the most downstream cylinder is kept at a value of 4 diameters so that the cylinders are in the wake-proximity region of each other. As the location of the middle cylinder is changed, the spacing between the centers of each two successive cylinders changes accordingly. The spacing between the axes of the upstream and middle cylinder x is used to define each arrangement. At $x = 2.00D$, the three cylinders are evenly spaced. The simulations include the spacings $x = 1.20D$ to $2.80D$ with a step of $0.2D$ in addition to the two extreme cases of $x = 1.05D$ and $2.95D$.

The laminar incompressible Navier–Stokes continuity and momentum equations, can be written in a dimensionless form as:

$$\nabla.\mathbf{u} = 0, \tag{1}$$

$$\frac{\partial \mathbf{u}}{\partial t} = -(\mathbf{u}.\nabla)\mathbf{u} - \nabla p + \frac{1}{\mathrm{Re}}\nabla^2\mathbf{u} \tag{2}$$

where $\mathbf{u}$ is the velocity vector normalized by the upstream flow velocity U_∞. The pressure p is normalized by ρU_∞^2. The Reynolds number is $\mathrm{Re} = \rho U_\infty D/\mu$ in a fluid of viscosity μ. Parameters used to characterize the interaction of the flow with the cylinders include the amplitude of the oscillating lift coefficient C_l, the time averaged drag coefficient $\bar{C_d}$, and the Strouhal number St defined as:

$$\mathrm{St} = \frac{fD}{U_\infty} \tag{3}$$

where f is the frequency of the oscillating lift force on the cylinder.

After simulating the flow around fixed cylinders, simulations are carried out to investigate the flow-induced vibration of the configuration of three unevenly spaced cylinders with the most downstream cylinder allowed to vibrate in the cross-flow direction. The spacing x between the upstream and the middle cylinders is limited to the range $1.40D \leq x \leq 2.20D$ for the simulations of the flow-induced vibration of the downstream cylinder, where flow patterns of interest and flow regime changes are expected to occur. The single-degree-of-freedom mass–spring–damper system is selected to model the motion of the most downstream cylinder. The moving cylinder is allowed only to move in the y direction under the fluid loading. The equation of motion of the cylinder, mounted on a basis providing the mass m, damping c, and the spring stiffness k per unit length of the cylinder span is:

$$m\ddot{y} + c\dot{y} + ky = \frac{1}{2}\rho U_\infty^2 D\hat{C_l} \tag{4}$$

where y, $\dot{y}$, and $\ddot{y}$ are the cylinder displacement, velocity, and acceleration; respectively. $\hat{C_l}$ is the time dependent lift coefficient which results from the calculated pressure distribution on the surface of the cylinder due to the coupling between the flow field and its motion. The unsteady cross-stream lift force acting on a cylinder in cross-flow is oscillating mainly due to the fluctuating pressures acting on the surface of the cylinder. The energy of the pressure fluctuation is typically concentrated to a band around the mean shedding frequency (Norberg, 2003). The vortex shedding frequency and the Strouhal number depend on the Reynolds number. The value of $\mathrm{Re} = 200$ is widely considered in the literature to be close to the upper threshold at which the flow around cylinders remains two-dimensional and laminar (Carmo and Meneghini, 2006; Papaioannou et al., 2006). Norberg (2003) also reported that at Reynolds numbers up to 6×10^3, the lift force spectra is similar to that of a sine wave at single frequency with random noise. At higher Reynolds number, the lift force spectrum is similar to a narrow band random noise function, indicating a broader range of frequencies. For laminar flow at a Reynolds number as low as 200, there would be no near-cylinder vortex dislocations which are responsible for intermittent major disturbances to the vortex shedding. Analysis of the lift force follows the hypothesis that the displacement has the same frequency as the lift force as suggested by Parkinson (1974). Results of a single cylinder and two tandem cylinders presented by Assi et al. (2010) show that harmonic approximation is reasonable. Bearman (2011) notes that the underlying assumptions in this hypothesis suggests that vortex induced vibration can be studied by harmonic forcing of the cylinder (e.g. Sarpkaya, 1979; Hover et al., 1998). Measurements by Morse and Williamson (2009) show that under controlled structural parameters, results obtained by forcing sinusoidal vibration of the single cylinder matches the free vibration response. Therefore, the fluid loading force can be modeled as a harmonic force oscillating with a frequency f and a phase shift ϕ with the tube displacement. The force coefficient in the motion direction, $\hat{C_l}$, is time dependent and is resolved into a time-average, $\bar{C_l}$, and an oscillating component of amplitude C_l. Since the gravitational body force is not present in the simulation plane, the time-average lift coefficient $\bar{C_l}$ is expected to cancel out. As a result, the displacement y of the cylinder has an amplitude A and can be modeled in the form:

$$y(t) = A\sin(2\pi ft)\,. \tag{5}$$

The dimensionless structure parameters are the solid to displaced fluid mass ratio m^*, and the damping ratio ζ, defined as:

$$m^* = \frac{4m}{\pi D^2 \rho}; \qquad \zeta = \frac{c}{2\sqrt{mk}}. \tag{6}$$

The structural natural frequency of the vibrating cylinder f_n, and the reduced velocity U_r are defined as:

$$f_n = \frac{1}{2\pi}\sqrt{\frac{k}{m}}; \qquad U_r = \frac{U_\infty}{f_n D}. \tag{7}$$

The current study aims to investigate the response of the most downstream cylinder at reduced velocities ranging from 2 to 30. The dimensionless structural parameters are selected as $m^* = 2.4$ and $\zeta = 0.0059$. The selected mass ratio and damping coefficient allow for comparison with other studies, matching the parameters used in other numerical studies (Borazjani and Sotiropoulos, 2009; Ahn and Kallinderis, 2006; Bao et al., 2011). For every configuration, the reduced velocity is the only parameter allowed to change. The six degree of freedom algorithm requires input of allowed motion directions, external force vector, and dimensional inertia m of the cylinder. In order to solve at different values of U_r and fix the selected values of Re, m^*, and ζ, the algorithm adjusts the dimensional values of f_n, k and c using Eqs. (6) and (7). The algorithm then calculates the time dependent external forces on the cylinder and its motion for each time step according to Eq. (4). In this explicit approach, the pressure distribution on the surface of the cylinder is calculated by the flow solver. The resulting forces on the cylinder surface are then conveyed to the structure solver. The algorithm used allows for six degrees of freedom,

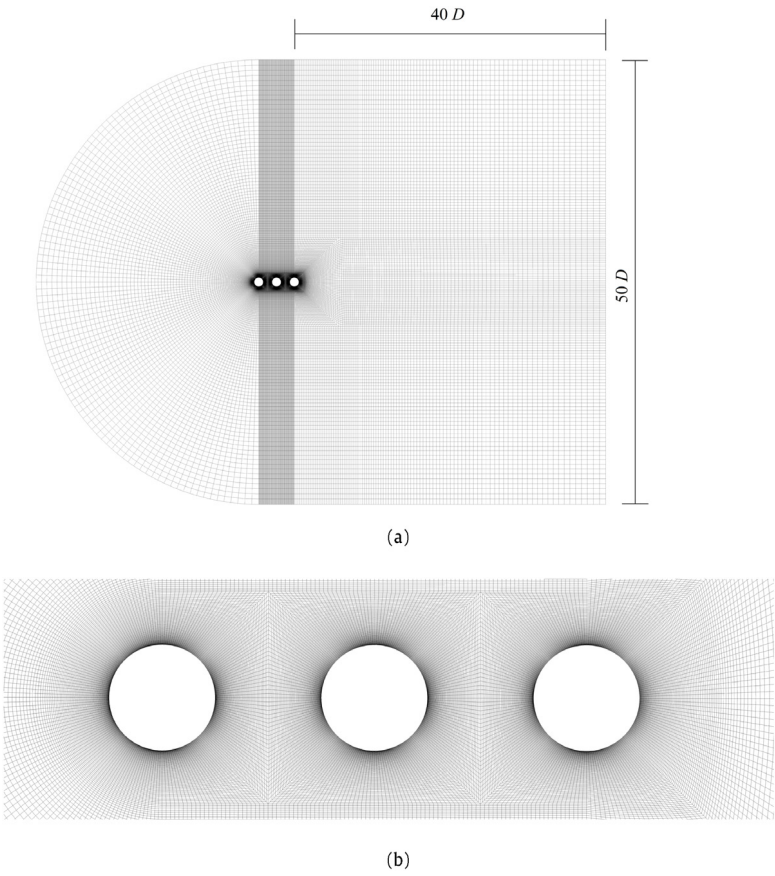


Fig. 2. (a) The computational domain and (b) the structured mesh around the three cylinders.

calculating displacements and rotations in space as result of forces and momentum in three dimensions. In this work, the cases studied are all constrained in five of the six allowed motion directions. Although it is more convenient in experimental studies to change U_r by allowing U_∞ to change resulting in a range of Reynolds number for each experiment, Hover and Triantafyllou (2001) measured the vibration response of a single cylinder and two tandem cylinders at a fixed value of Re $= 3 \times 10^4$. They were able to physically adjust the natural frequency of the structure while keeping the flow velocity constant by means of a control system. Their results follow the same behavior of other studies where Reynolds number changes. This method is used in many numerical studies (e.g. Ahn and Kallinderis, 2006; Carmo et al., 2011) as it allows for isolating the effect of Reynolds number on the vibration response of the oscillating cylinder.

For the flow around a single cylinder, Farrant et al. (2000) suggested that a computational domain with 16D upstream, 14D downstream, and 10D on either sides of the cylinder would provide a reasonable compromise between accuracy and computational cost. In the current study, the domain in Fig. 2 extends 25D upstream, 25D on either sides, and 40D downstream. The flow domain is meshed into a two-dimensional quadrilateral structured grid. The number of elements in the domain was around 1.1×10^5, varying slightly depending on the arrangement. A mesh sensitivity test verified that increasing the number of elements does not influence the lift coefficient amplitudes on the three cylinders. The domain in the upstream side takes the shape of a semicircle to save computational cost and optimize the quality of the mesh elements. The wall of each cylinder is divided into 200 elements along its circumference. A structured inflation zone is used on the walls of the three cylinders to accurately resolve the flow boundary layer. The first element on the cylinder wall is of height 0.001D, and the elements slowly increase in size at a growth ratio of 1.025. Farther away from the cylinders where no fluid–structure interaction takes place, the largest elements are of a maximum size of 0.5D. Uniform velocity boundary condition (i.e., $u = 1$, $v = 0$) is imposed at the upstream and the side boundaries of the domain. At the cylinder wall, no slip condition (i.e., $u = v = 0$) is applied. An incompressible outflow condition is imposed at the downstream outlet.

The pressure–velocity coupling scheme used is pressure implicit with splitting of operator (PISO). A second order upwind spacial discretization scheme of the convective terms is used for its high stability and accuracy compared to the lower-cost first order scheme. A Green–Gauss cell based discretization scheme is used for the diffusion terms for its stability at the selected value of Reynolds number. The transient term is discretized using a second order scheme for the simulations with no cylinder motion. However, a first order transient scheme is used when simulating the motion of the cylinder because

Table 1
Force coefficients and Strouhal numbers for flow around a single cylinder at Re = 200.

	$C_{l,rms}$	$\bar{C}_d$	St
2D simulations			
Liu et al. (1998)	0.49	1.31	0.192
Farrant et al. (2000)	0.50	1.36	0.196
Meneghini et al. (2001)	0.50	1.30	0.196
Lam et al. (2008)	0.43	1.32	0.196
3D simulations			
Zhang and Dalton (1998)	0.48	1.32	0.178–0.198
Current study	0.48	1.35	0.196

of its compatibility with the dynamic mesh models. To allow for cylinder motion, location of cylinder nodes is recalculated using the node diffusion Laplace smoothing method with a diffusion parameter of 0.70, which was found to ensure stability throughout the simulations. To validate the model, a simulation of the vortex shedding around a single cylinder was carried out, and the results of the root mean square of the lift coefficient, average drag coefficient, and Strouhal number are shown in Table 1. It is clear from Table 1 that a good agreement is obtained with other two and three dimensional simulations at the same Reynolds number.

For each arrangement, the simulation runs are initialized by the steady solutions of the flow field. The transient simulations are performed at a dimensionless time step $\Delta tU/D$ of 0.05 to ensure a reasonable compromise between computational cost and accuracy as recommended by Farrant et al. (2000). One vortex shedding cycle is simulated in at least 100 time steps for any configuration. The time step was varied to check the time step influence on the structural and added fluid damping. Using smaller dimensionless time steps of 0.005 and 0.001 did not have any significant influence on the ratio of the total system damping to the critical damping. Subsequently, the simulation runs for 5×10^4 time steps, with 10 iterations in each time step, to ensure full statistical convergence. This large number of time steps is selected to allow for a stable final solution. The solution at 5×10^4 time steps is used as an initial solution for the dynamic mesh case when the flow-induced vibration simulations are initiated. Section 3 discusses the results of the simulations when the three cylinders are rigidly fixed. After that, Section 4 will discuss the results when the downstream cylinder is allowed to oscillate.

3. Flow around three rigidly fixed cylinders

Fig. 3 shows the amplitude of the fluctuating lift coefficient on the three cylinders for different locations of the middle cylinder. Each figure is divided into two figures as the range of locations is divided into two regions with orders of magnitude difference in the lift force. When the middle cylinder is at x/D of 1.60 and 1.80, the value of C_l on the upstream cylinder is an order of magnitude higher than its value when the middle cylinder is located at any other location. This trend is observed for the second and third cylinders as well, and the lift force increases nearly 100 times on the middle cylinder, and 8 times for the downstream cylinder. The excessive increase of the fluctuating lift force on the middle cylinder suggests that the cylinder becomes subject to a significantly different flow regime. For the locations where low values of C_l are observed, the lift coefficient increases as the middle cylinder moves closer to the most downstream cylinder. When the gap between the middle cylinder and the downstream cylinder is smaller than 1.4 diameters (i.e. $x/D = 2.6$), the lift coefficient starts to decrease. The value of the fluctuating lift on the upstream and middle cylinders in these cases are nearly similar, while the fluctuating lift on the downstream cylinder is an order of magnitude higher. On the other hand, for the cases of $x/D =$ 1.60 and 1.80, the fluctuating lift on the middle and downstream cylinders are of the same order of magnitude, while the fluctuating lift on the upstream cylinder is much lower. In all cases, the fluctuating lift force on the downstream cylinder is higher than that on the upstream and middle cylinders.

Abrupt changes of the mean drag coefficient and Strouhal number are also observed for the same middle cylinder locations, i.e., $x/D = 1.60$ and 1.80. Fig. 4 shows the time-averaged drag coefficient on the three cylinders. Aside from the higher values at $x/D = 1.60$ and 1.80, the drag coefficient on the upstream cylinder decreases slightly as the gap between the upstream and middle cylinder gets wider. The drag coefficient is negative on the middle cylinder and positive on the downstream cylinder. Moreover, Fig. 4b shows that the middle cylinder experiences the minimum drag when the cylinders are equally spaced, i.e., $x/D = 2.00$.

Fig. 5a shows the spectrum of the lift force on the three cylinders at three different locations of the middle cylinder. The higher frequencies in the oscillating lift force are weaker than the main component by at least an order of magnitude. For the three cylinders, the peak oscillating lift force is confined at the main frequency which is strongest for the middle location of $x/D = 1.80$. It can be seen that the harmonics of the lift force for the case of $x/D = 1.80$ are relatively stronger than the two other cases. Fig. 5b shows the Strouhal number, calculated from the frequency of the fluctuating lift coefficient, which is found to be the same for the three cylinders. The figure shows that the Strouhal number ranges between 0.150 and 0.155 for all middle cylinder locations, except the two positions of $x/D = 1.60$ and 1.80 where it drops significantly nearly to 0.10. This jump is due to changes in the flow pattern as will be discussed later.

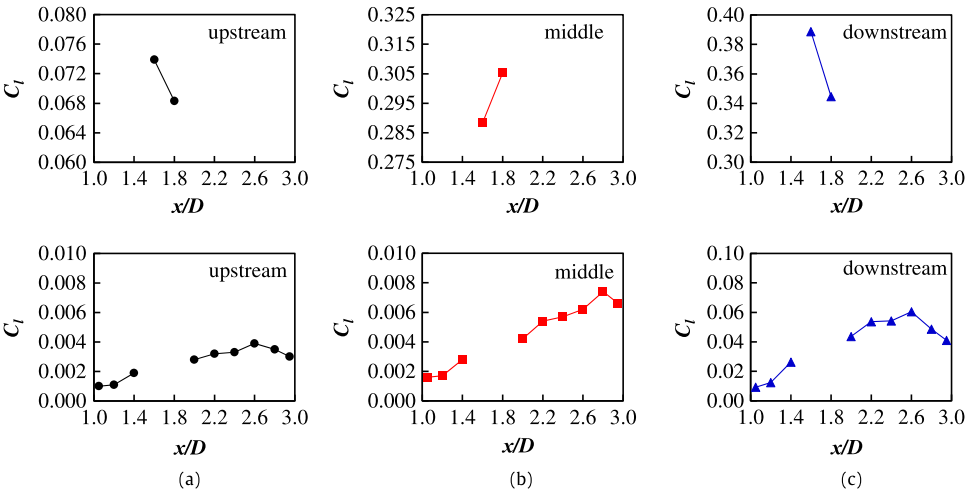


Fig. 3. Fluctuating lift coefficient on the (a) upstream, (b) middle, and (c) downstream cylinders for different locations of the middle cylinder.

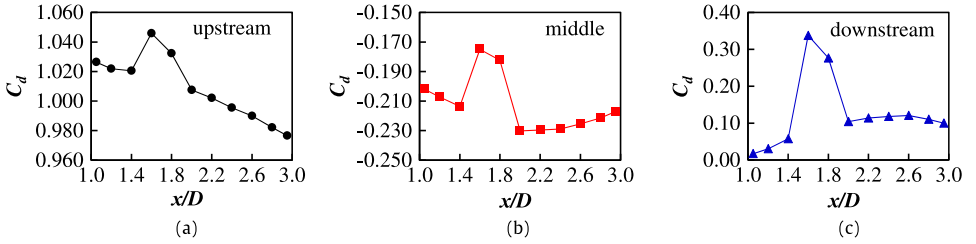


Fig. 4. Time-averaged drag coefficient on the (a) upstream, (b) middle, and (c) downstream cylinders for different locations of the middle cylinder.

Fig. 6 shows contours of instantaneous normalized vorticity in addition to flow streamlines at five instants during one shedding cycle of period T. The figure shows two cases, at $x/D = 1.60$ and 2.00 in Fig. 6a, and 6b; respectively. The values of lift coefficient at $x/D = 1.60$ are significantly higher than the other case of $x/D = 2.00$, and the Strouhal number is significantly lower. The five points constitute half a shedding cycle, and the other half is a mirrored version of these instants due to symmetry. The figures show significant differences in the flow characteristics between the two cases. The five instants for $x/D = 1.60$ in Fig. 6a show that a band of streamlines pass through the gap between the middle and downstream cylinders. Vorticity contours for the same case show rolling shear layer flow in the same location. Higher vorticity is observed on the wall of the most downstream cylinder and vortices start to evolve and dispatch downstream. The upstream stagnation point on the wall of the most downstream cylinder oscillates significantly due to vortex formation in the gap leading to stronger vortices. On the other hand, the five instants for $x/D = 2.00$ in Fig. 6b show symmetric circulating flow in the gap between the upstream and middle cylinders as well as the gap between the middle and downstream cylinders. Moreover, the stagnation points on the three cylinders do not oscillate significantly. Vortex shedding and rolling of the shear layers is only observed downstream of the most downstream cylinder. The occurrence of reattachment on the downstream cylinder causes higher force coefficients and lower Strouhal numbers.

Fig. 7 shows the time-averaged pressure coefficient distribution on the surface of the middle and downstream cylinder, taking the upstream stagnation point as the reference for the angle θ. The integral of the time-averaged pressure over the cylinder results in the time-averaged force exerted by the fluid. The distribution is symmetric around the streamwise axis of each cylinder, resulting in an average lift force of $\overline{C_l} = 0$. Therefore, data over only one half of the cylinder surface is plotted. Moreover, the differences of the pressure distribution when the middle cylinder location is varied explain the trend of the mean drag force on the middle and downstream cylinders, shown in Fig. 4. It can be seen that the cases of middle cylinder locations $x/D = 1.60$ and 1.80 are distinguishable among all other cases by a different pressure distribution. This different pressure distribution indicates a significant change in the flow features adjacent to the surface of the middle and downstream cylinders, most notably the displacement of the flow separation points further upstream. Moreover, the different flow features for the two cases of $x/D = 1.60$ and 1.80 can be attributed to the separation of vortices in the gap between the middle and the downstream cylinders.

Fig. 8 shows the oscillations of the lift force on the middle and downstream cylinders versus the lift force on the upstream cylinder. The elliptic plot of cycles is symmetric around the origin indicating that the cycle can be described using only one

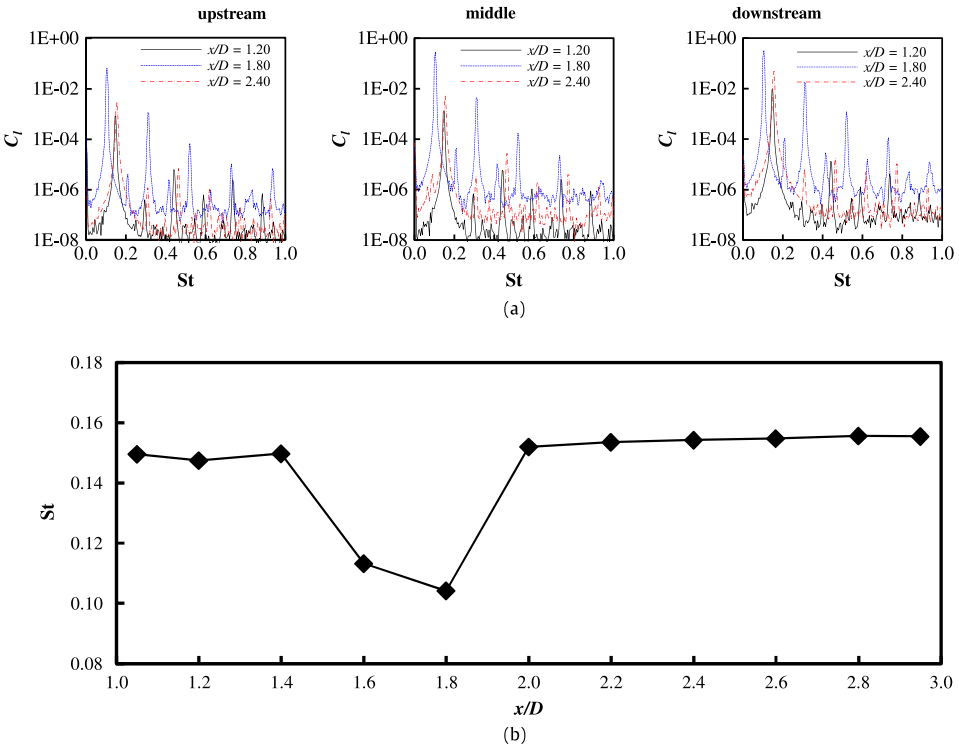


Fig. 5. (a) Power spectral density and (b) Strouhal numbers of the fluctuating lift force on the three cylinders for different locations of the middle cylinder.

half and the other half is equivalent to its mirrored image. The magnitude of the lift force on the three cylinders is much higher in the case of $x/D = 1.60$ as previously noted. For the middle cylinder location of $x/D = 2.00$, the lift forces on the three cylinder are in phase which indicates that the vortex shedding on the three cylinders occurs in the same direction at any instants of time. For the other case of $x/D = 1.60$, the lift force on the downstream cylinder is out of phase with the lift force on the upstream and middle cylinders indicating that the vortex in the gap between the middle and downstream cylinder is out of phase with the vortex shed at the downstream cylinder.

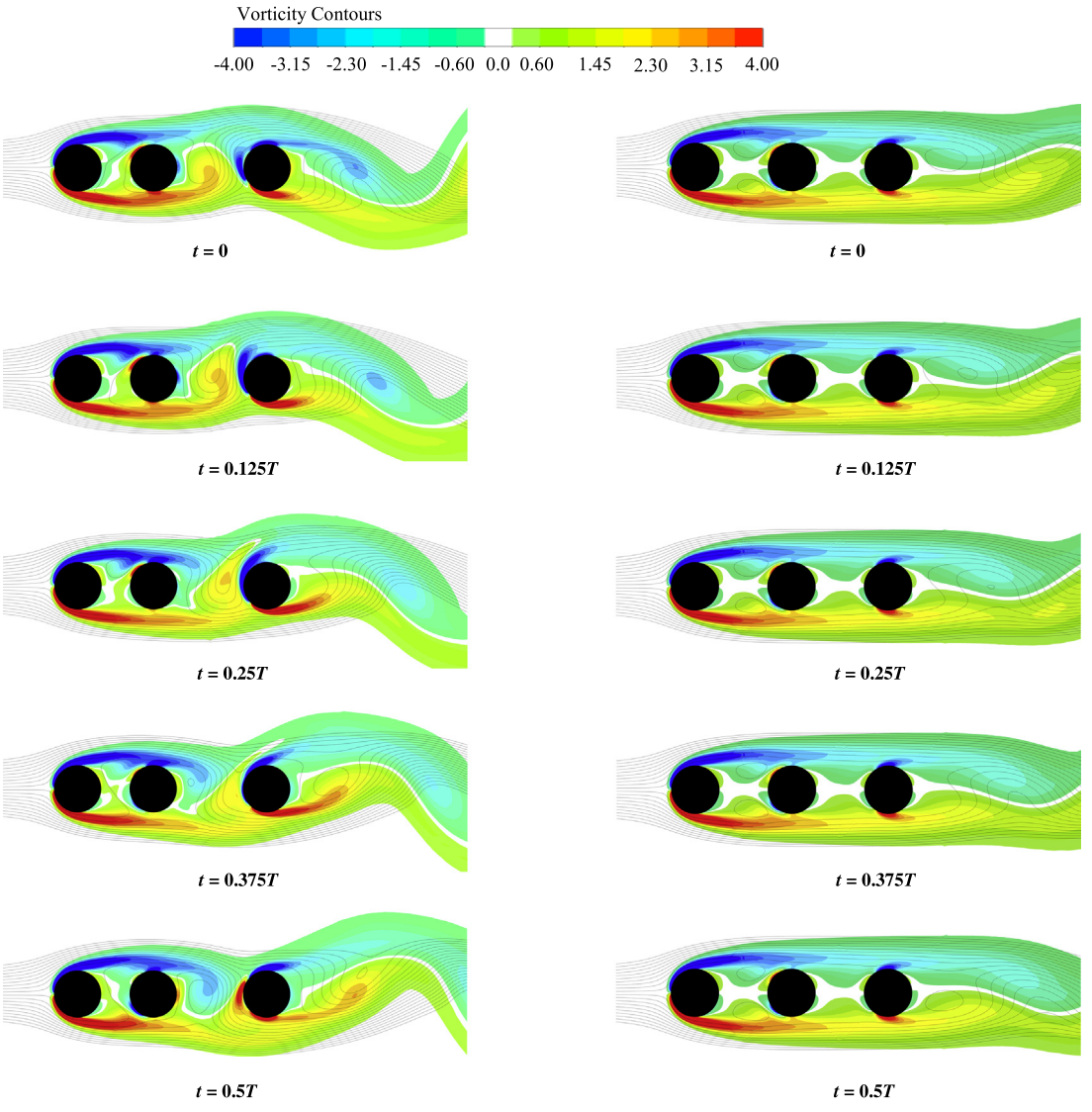
Fig. 9a shows the normalized vorticity contours around the three cylinders at two locations of the middle cylinder, $x/D = 1.60$ and 2.00. The street of vortices that develop downstream of the cylinders shows notable differences. The vortices in the case of $x/D = 1.60$ are larger and have higher vorticity magnitudes associated with the higher oscillating lift forces on the downstream cylinder. To investigate if the vortex formation length is different in the two cases, the distribution of the normalized axial component of velocity u_x/U_∞ is plotted against the distance downstream from the most downstream cylinder x_{ds} in Fig. 9b for the two cases. The vortex formation length defined as the downstream length at which the value of u_x/D is negative is $0.634D$ for the case of $x/D = 1.60$. The vortex formation length for the other case, $x/D = 2.00$, is $1.772D$. The significant differences in the vortex formation lengths between the two distinct patterns suggest an important role for the flow upstream of the most downstream cylinder.

In conclusion, the flow around three fixed inline cylinders is sensitive to the spacing between them. Different flow patterns can occur due to slight changes in the gaps between the cylinders, resulting in different Strouhal numbers and lift and drag coefficients indicating that these interesting flow patterns cannot be inferred from the cases of two or three inline cylinders with even spacing. It is important to investigate the effect of these different flow patterns on the flow-induced vibration response of three inline cylinders with uneven spacing.

4. Flow-induced vibration of the downstream cylinder

This section discusses the results of the second phase of this work, in which the downstream cylinder is attached to an elastic base. The flow-induced vibration response of the most downstream cylinder for uneven spacing of the three cylinders is presented. In all of the discussed cases, only the most downstream cylinder is allowed to oscillate in the transverse direction in reaction to the structure and fluid forces.

In order to validate the numerical model, the single-degree-of freedom vibration of a single cylinder was simulated. Simulations were performed at two different Reynolds numbers, and the structural parameters of $(m^* = 2.55, \zeta = 0)$ were



(a) x/D = 1.60. (b) x/D = 2.00.

Fig. 6. Instantaneous streamlines and normalized vorticity contours through half a cycle for the cases of (a) $x/D = 1.60$ and (b) $x/D = 2.00$ when all three cylinders are fixed.

selected to match the parameters used in other numerical studies (Borazjani and Sotiropoulos, 2009; Ahn and Kallinderis, 2006; Bao et al., 2011). Carmo and Meneghini (2006) used values of ($m^* = 2.0$, $\zeta = 0.007$) and their model gives a good agreement with the results of the current model, suggesting that the maximum amplitude of vibration is not sensitive to small changes in structural parameters. Fig. 10 shows a good agreement of the cylinder response. It also shows that the maximum amplitude calculated at the same structural parameters did not change significantly with the change in Reynolds number, which agrees with the observation of Govardhan and Williamson (2006) for a single cylinder in laminar flow. The results at Re = 200 agrees well with the results of Borazjani and Sotiropoulos (2009) and shows a narrower lock-in range. These results show that the model captures the vortex-induced vibration response and accurately describes the interactions between the flow and the flexible cylinder.

Fig. 11 shows the transverse flow-induced vibration response of the most downstream cylinder when the three cylinders are equally spaced. Fig. 11a shows the normalized amplitude of the displacement and the lift coefficient behavior at the same range of U_r. For $U_r < 4.0$, the lift coefficient and the amplitude of the displacement have negligible values. The lock-in region occurs for $4.5 \leq U_r \leq 10$, where both the lift coefficient and the amplitude of oscillation increase to a maximum value, then start to decrease again. The behavior at $U_r \geq 10$ is different. The amplitude of cylinder oscillation starts to decrease from

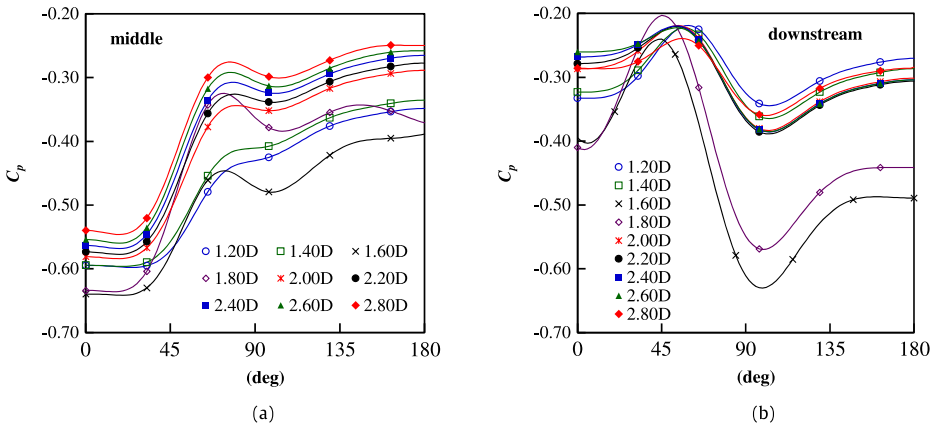


Fig. 7. Time-averaged pressure coefficient on the surface of the middle and downstream cylinders for different locations of the middle cylinder.

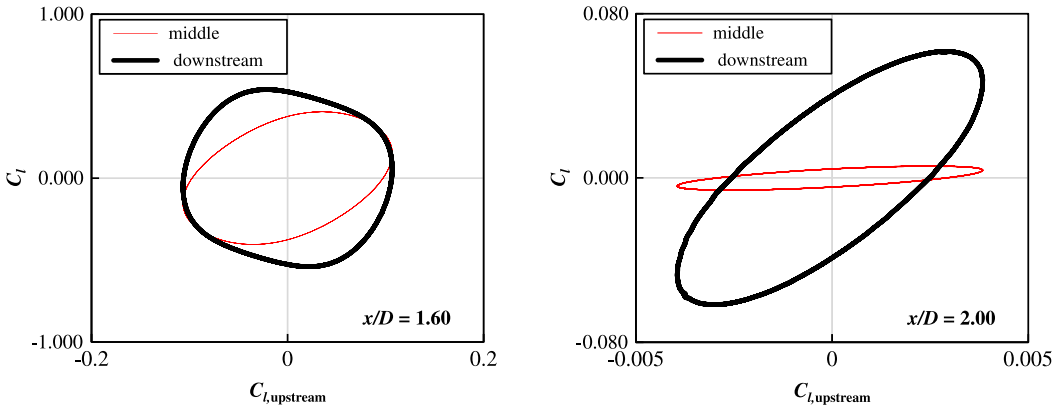


Fig. 8. Phase portraits of lift forces on the middle and upstream cylinders relative to the lift force on the upstream cylinder for the two cases of $x/D = 1.60$ and $x/D = 2.00$.

its maximum value of 1.0D gradually. At higher reduced velocities, the value of the oscillation amplitude is asymptotic to a value of 0.5D. However, the lift coefficient decreases at a much higher rate after it reaches its maximum value of 1.5. It reaches a minimum value of 0.05 at $U_r = 8.5$ before it starts to increase again towards a value slightly higher than 0.5. In the range where the lift force is notably low, the favorable phasing causes high oscillation amplitudes for lower lift coefficient. The lift coefficient then increases to drive the displacement when the phase angle is slightly lower than 180°.

Fig. 11b demonstrates the oscillation frequency f normalized by the structure natural frequency f_n. It also shows the phase angle between the displacement and the lift force ϕ as a function of the reduced velocity U_r. The normalized frequency of oscillation can be divided into three ranges of U_r, at each range the frequency increases linearly with a different rate. Such an abrupt change in the frequency of vortex shedding without corresponding changes in geometry or flow velocity indicates that the mechanism of energy transfer is different for the three regions. For $U_r \leq 4.5$, a higher rate of increase in frequency is observed, while the displacement and lift force are nearly in phase. In this range, the phase shift between displacement and lift increases indicating a higher energy transfer between the structural and fluid forces. At $U_r = 7.5$, the frequency coincidence occurs and $f/f_n = 1$ causing the phase between the displacement and the lift force to jump by 180°. At $U_r \geq 10$, the phase shift remains at 180°, and the frequency starts to increase at a higher rate.

Fig. 12 shows the instantaneous vorticity contours and the streamlines at five different positions of the downstream cylinder during half an oscillation cycle. The figure shows the flow structure for the same two locations of the middle cylinder shown in Fig. 6 to investigate the effect of the downstream cylinder motion on the flow around the cylinders. The five instants are shown at the reduced speed $U_r = 6.0$ which causes the maximum displacement amplitude of nearly $A = 1.00\ D$ for both cases. The five instants in Fig. 12a for $x/D = 1.60$ show that the position of the cylinder as well as its motion direction influences the flow around the cylinders. The flow when the downstream cylinder oscillates is notably different than the flow around the three fixed cylinders shown in Fig. 6. The shear layers of the middle cylinder are allowed to roll and shed vortices in the gap between the middle and the downstream cylinders. The motion of the downstream cylinder creates higher vorticity and noticeably larger vortex size compared to the same case in Fig. 6. In addition, the flow around the

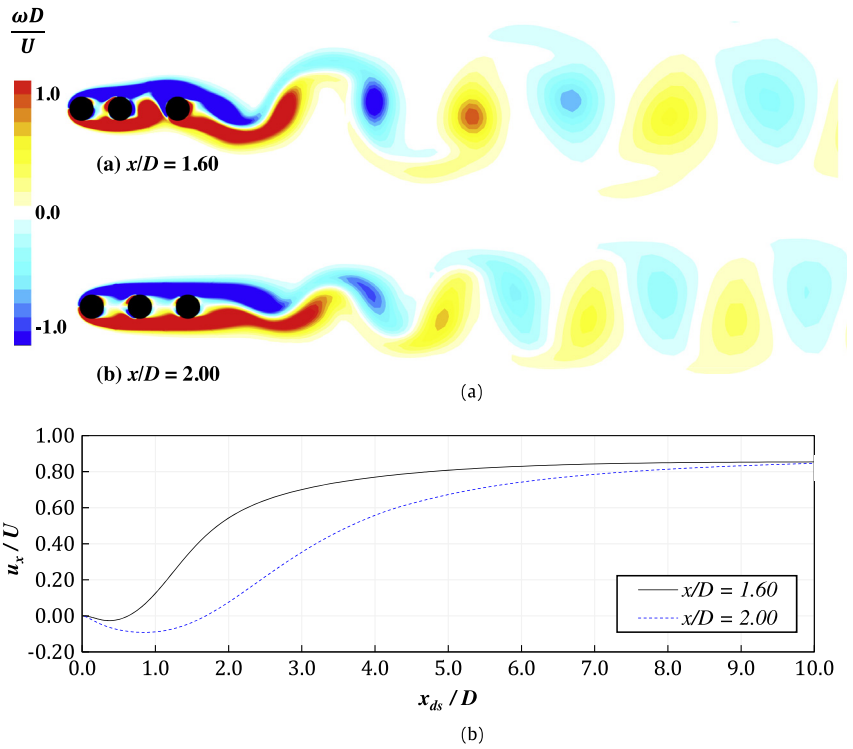


Fig. 9. (A) The vortex street and (B) the normalized streamwise velocity downstream of the three inline cylinders for the two cases of $x/D = 1.60$ and 2.00.

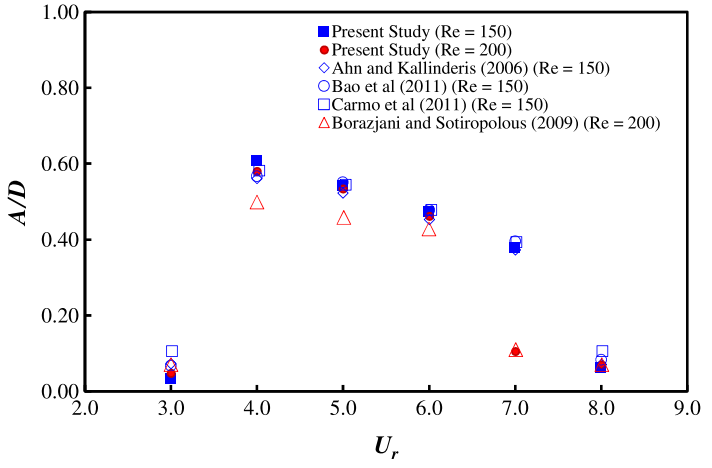


Fig. 10. Vortex-induced vibration response of a single cylinder for Re = 150 and 200, at structural parameters of $m^* = 2.55$ and $\zeta = 0$ compared with other results in literature.

cylinders for both cases in Fig. 12a and 12b show similar characteristics, despite their different flow patterns in Fig. 6a and 6b; respectively. When the middle cylinder is located at $x/D = 1.60$, the size of the circulating zones between the upstream and middle cylinder is slightly smaller than their size for the case with $x/D = 2.00$. The flow around the downstream moving cylinder is remarkably similar. The changes introduced by the motion of the most downstream cylinder dominates the flow around the three cylinders, noting that the displacement amplitude of the two cases is nearly the same.

Fig. 13a presents a comparison of the arrangement discussed in Fig. 11 with the cases of a single cylinder oscillating due to vortex shedding, and the case of two tandem cylinders at a spacing of $x/D = 2.0$. The discussed case of an elastically-mounted downstream cylinder in the wake of two fixed upstream cylinders experience higher amplitude of oscillation than the other two cases. At higher reduced velocities, the case of a single cylinder oscillates at a negligible amplitude, and the flow-induced

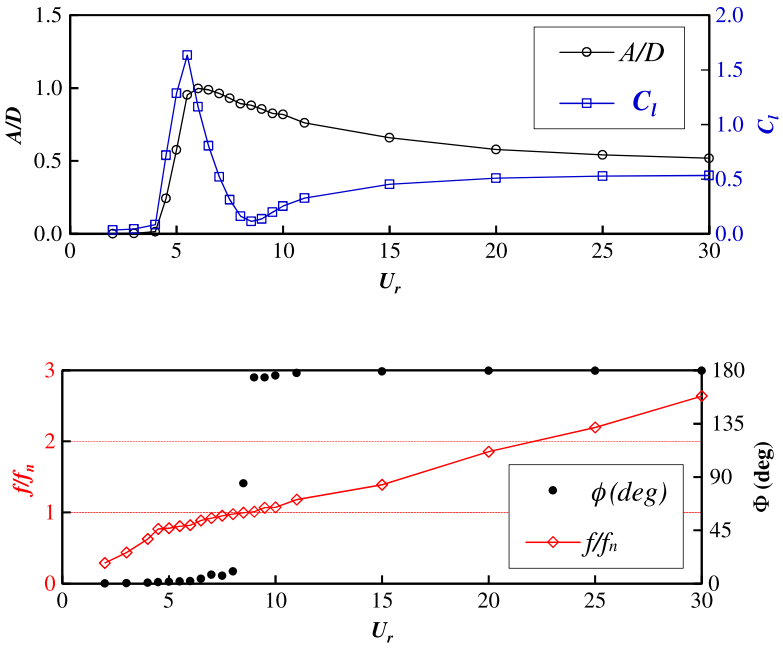


Fig. 11. Flow-induced vibration response of the downstream cylinder for three evenly-spaced cylinders.

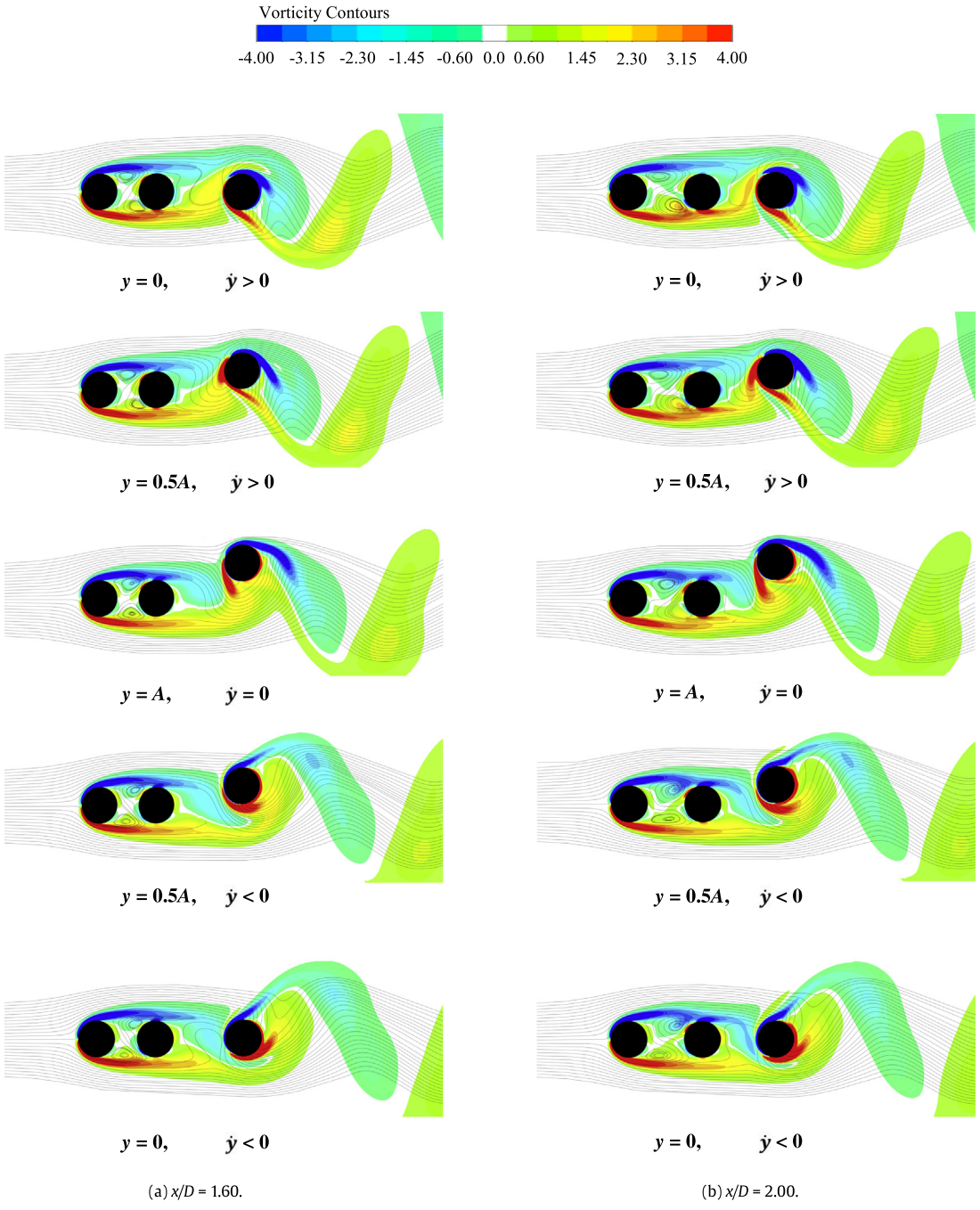
vibration response agrees well with the results of other investigations in literature (e.g. Khalak and Williamson, 1997; Assi et al., 2010; Carmo et al., 2011). On the other hand, the amplitude at reduced velocities as high as $U_r = 30$ is notable for the case of two tandem cylinders, and is significantly higher for the case of three cylinders. The range of lock-in, at which significantly higher amplitudes are observed, is broader and occurs at a higher reduced velocity as the number of cylinders increases.

Fig. 13b shows the normalized frequency of oscillation for the same three cases. The lock-in range is found to be broader as the number of cylinders increases. The frequency of oscillation for the cases of a single cylinder and two tandem cylinders exhibits a higher rate of increase due to the higher Strouhal number. Fig. 13c shows the effect of the middle cylinder location on the flow-induced vibration of the downstream cylinder when the cylinders are unevenly spaced. No significant change is observed for the maximum amplitude which reaches nearly $A/D = 1.0$ for all simulated cases. However, a significant change is seen at higher reduced velocities, where the case of even spacing results in the highest displacement amplitude. The highest amplitude of oscillations is detected for the case of even spacing, i.e., $x/D = 2.0$. At higher or lower values of x/D, the amplitude is lower than the case of equally spaced cylinders at higher reduced velocities.

The phase portraits in Fig. 14 are created by plotting the displacement against the oscillating lift force during complete cycles of oscillations. These phase portraits show various features of the dynamic response of the system. For the system of a simple harmonic oscillator, the orientation of the major axis of the curve is related to the phase between the displacement and the lift force. The area enclosed by the curve represents the energy exchanged between the structure and the flow field. Fig. 14 compares the cases of a single cylinder, three inline cylinders at $x/D = 1.60$, and $x/D = 2.00$. Complete cycles for each case are plotted in the y/D - C_l plane at three reduced velocities, $U_r = 2.00$, 6.00, and 10.00. All figures are symmetric with respect to the origin, confirming that the motion can be inferred from one half of a cycle.

At the low reduced velocity of $U_r = 2.00$, the three different configurations of cylinders lie in the first and third quadrants, indicating that the moving cylinder displacement is in phase with the oscillating lift force. The displacement has a relatively low amplitude, and the curve is very close to a straight line demonstrating that the phase angle is close to zero. The energy supplied by the flow to the structure, represented by the area enclosed inside the cycle, is negligible for the three configurations, resulting in the low displacement.

As the reduced velocity is increased to $U_r = 6.00$ and the frequency increases at a much lower rate with U_r, the phase portraits show interesting features. The amplitude of both the lift force and the displacement is significantly higher than their values at the lower reduced velocities of $U_r = 2.00$. The significant difference between the case of a single cylinder and the two other cases at the reduced velocity of $U_r = 6.00$ unveils an important feature of the dynamic response of the configuration of three inline cylinders. The response of a single cylinder is one closed curve with one anticlockwise ring. On the contrary, the portraits for the downstream cylinder of three inline cylinders consists of three distinct areas enclosed by the cycle. The plots are still symmetric and nearly in-phase. The two enclosed areas at the edges of the cycle curve are oriented clockwise and occur at high amplitudes when the cylinder is outside the wake of the two upstream cylinders. The cycle does not take an elliptic shape which defines a single frequency system. Rather, the periodic interactions of the displacement and



(a) x/D = 1.60. (b) x/D = 2.00.

Fig. 12. Instantaneous streamlines and normalized vorticity contours through half a cycle of cylinder oscillation for the cases of (a) $x/D = 1.60$ and (b) $x/D = 2.00$.

the lift force occur at a range of frequencies. At high values of the displacement, positive energy is supplied by the flow field to the cylinder kinetic energy. On the other hand, the middle ring is clockwise and occurs when the cylinder is located in the wake of the two upstream cylinders. This indicates that the cylinder loses energy to the flow field when the displacement is low. The net energy input from the flow field to the cylinder over the cycle is always positive to provide the necessary forcing against the structural damping by the fluid. The negative energy taken out of the cycle when the cylinder lies inside the wake of the upstream objects indicates that the dynamic lift force on the cylinder at this region is a stabilizing force that acts to stabilize the motion of the cylinder to its equilibrium position. The kinetic energy of the cylinder at this region is higher than the decrease that the force is able to cause. Thus, the motion continues and moves out of the wake where energy

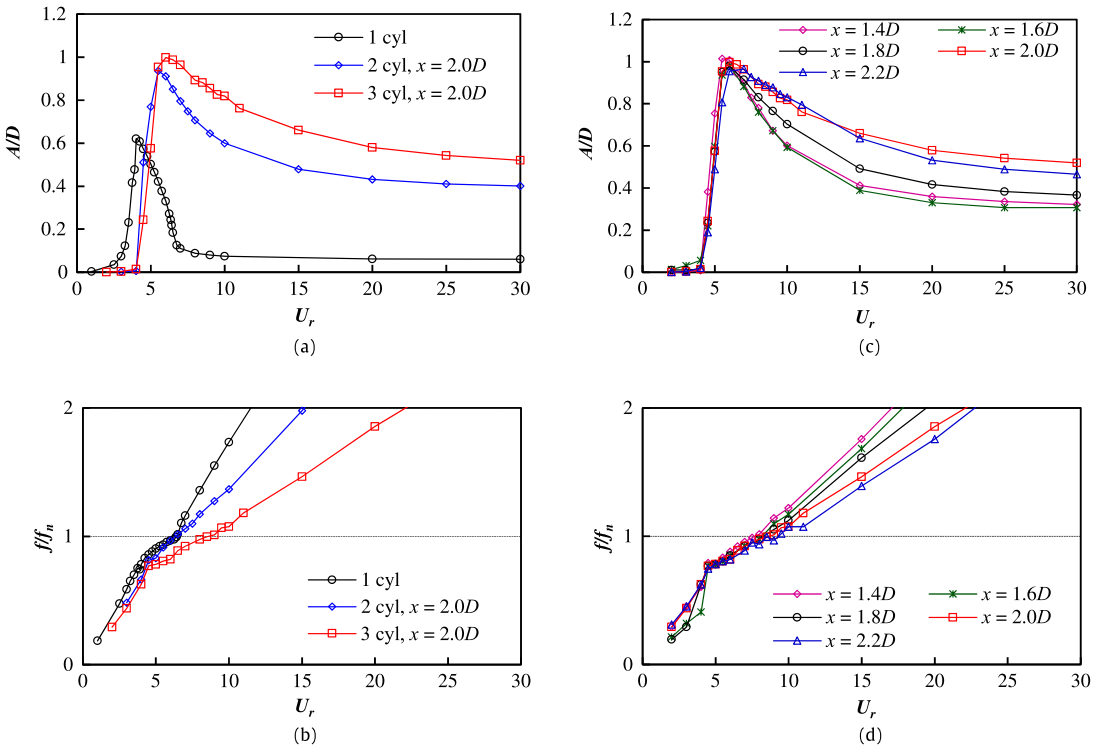


Fig. 13. Amplitude and frequency of the vortex induced vibration of the downstream cylinder in three inline cylinders, (a,b) compared with the cases of a single cylinder and two tandem cylinders, and (c,d) showing the effect of cylinder uneven spacing.

is supplied to its motion to compensate for this deficit. The stabilizing force inside the wake originates from the deficit in the static pressure in the wake. The static pressure is lowest at the center of the wake and increases outside the wake. The effect of the upstream wake, therefore, is responsible for the difference in the dynamic response shown in Fig. 13 for the case of a single cylinder.

At the higher reduced velocity of $U_r = 10.00$, the amplitude of the single cylinder oscillations is reduced, and the energy exchange decreases back to levels similar to those at low reduced velocity. The rate of increase of frequency with U_r for this case is also higher than the case for $U_r = 6.00$. This suggests that frequency of oscillation is dominated by the mechanism of energy transfer between the fluid and the cylinder. On the other hand, the cycle is oriented at the second and fourth quadrant of the y/D - C_l plane, indicating that the lift force and the displacement are out of phase. For the case of three inline cylinders, the amplitude is still significant, as shown before in Fig. 13. The lift force and the displacement for the two cases at $x/D = 1.60$ and 2.00 are out of phase. The higher amplitudes for the latter case is associated with lower lift force amplitudes, and with higher energy exchange, both positive and negative, between the flow field and the structure. The mechanism responsible for the oscillations of a single cylinder is related to the frequency of the vortex shedding on the cylinder. However, the case of three cylinders is dominated by the effects introduced by the presence of the two upstream cylinders and their spacing.

In light of the difference spotted in the plots in Fig. 14, the streamlines in Fig. 12 can help understand the way the wake interacts with the cylinder for the same two cases of $x/D = 1.60$ and 2.00. When the cylinder is at its maximum velocity, it is located at the center of the upstream wake and the streamlines can be seen to form a vortex at its upstream surface. The flow that separated at the upstream cylinders passes at the two sides of the cylinder. On the other hand, different flow features can be observed when the cylinder reaches its maximum displacement. At this location, streamlines pass through the gap between the fixed middle cylinder and the moving downstream cylinder. The flow velocity through this gap decreases the static pressure and creates the force that pushes the cylinder to continue the cycle. Therefore, the flow through this gap accounts for the main effect of the wake which explains the high oscillation amplitudes at high reduced velocities. At higher reduced velocities, the ratio between the vortex shedding on the moving cylinder and the structural resonance frequency diverges from the value of $f/f_n = 1.0$ at resonance. In contrast, higher flow velocities through the gap create higher pressure deficit and thus provide higher lift force on the cylinder. The two opposing mechanisms account for the gradual decrease of the amplitude seen in Fig. 11.

Fig. 13d shows the effect of uneven spacing on the normalized frequency of oscillation. As the reduced velocity increases, the normalized frequency of the downstream cylinder oscillation increases differently depending on the location of the middle cylinder. When the middle cylinder is located closer to the downstream cylinder, the frequency of oscillations is lower at each reduced velocity. Fig. 13d also shows that for each configuration, there are three ranges that can be distinguished by

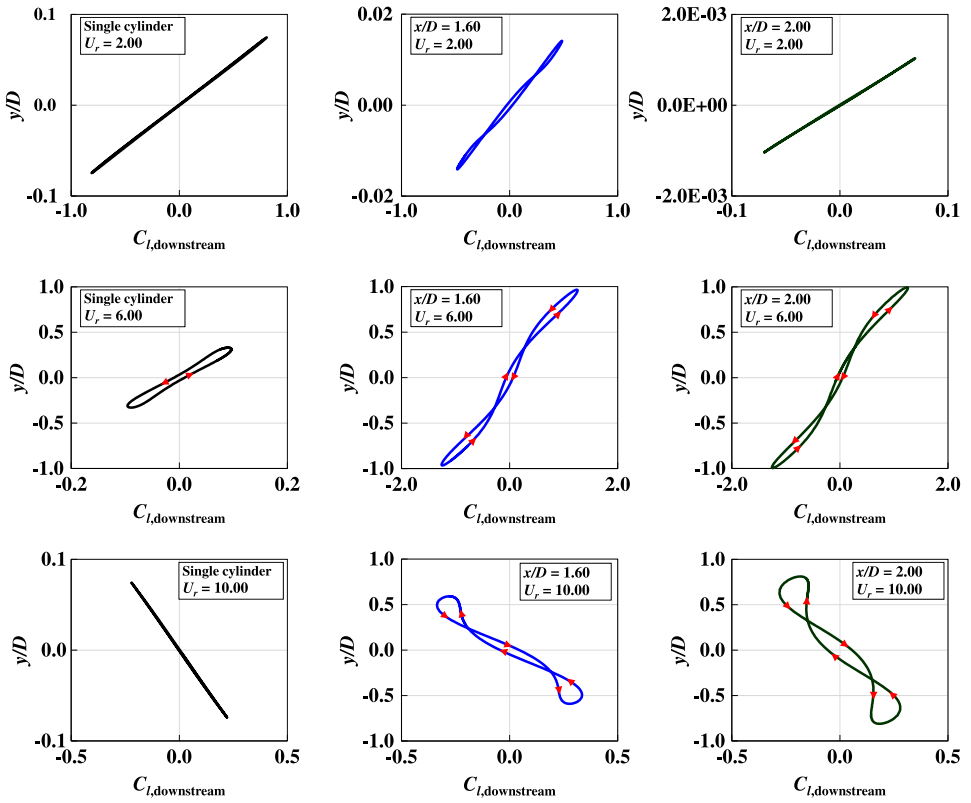


Fig. 14. Phase portraits of displacement and lift coefficient for a single cylinder, three cylinders with $x/D = 1.60$, and three cylinders with $x/D = 2.00$ at three different reduced velocities.

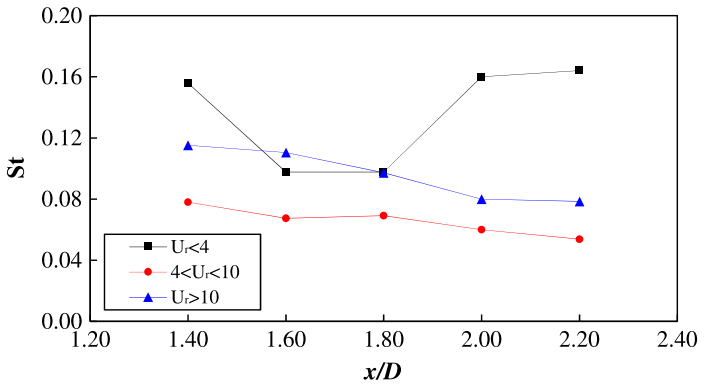


Fig. 15. Strouhal number of the fluctuating lift force in the three ranges of reduced velocities for different locations of the middle cylinder.

the slope of the frequency f/f_n. The lock-in region extends between U_r of 4 to 10, where f/f_n slope is lower than that observed at values of U_r outside the lock-in region. The effect of the locations of the middle cylinder on the slope of the frequency at the three regions can be seen in Fig. 15. Strouhal numbers in this graph are obtained by calculating the normalized slope of the frequency at the three regions. For the first range at very low reduced velocities, the location of the middle cylinder has a significant influence on the Strouhal number. For x/D of 1.60 and 1.80, a significant decrease in the value of St to 0.10 is observed. No such jump is observed for the two other regions, whose Strouhal numbers decrease as the middle cylinder is moved closer to the downstream cylinder. The abrupt jump in St for the cases of $x/D = 1.60$ and 1.80 is detected only before the onset of the lock-in region. For the same two cases, Fig. 5 shows a similar jump in Strouhal number when the three cylinders were fixed. This suggests that the low amplitude of oscillation does not change the wake patterns from the case of three fixed cylinders. Consequently, the Strouhal number is sensitive to the location of the middle cylinder before the onset of lock-in region. When significant amplitudes of oscillation are observed, the Strouhal number values still show a

dependency on the location of the middle cylinder, but there is no indication of changes in flow patterns. This behavior shows that the motion of the downstream cylinder has a strong influence on the flow patterns around the three inline cylinders.

It is interesting to note the occurrence of high amplitudes of oscillations and the significant increase in the lift force from the case of a single cylinder over a wide range of reduced velocities. This suggests that the configuration of three inline cylinders is a potential candidate for use in low-velocity energy harvesting devices such as those using vibrating long cables offshore. Such devices can allow for more efficient use of the low energy densities usually encountered in wind or current speeds. Devices with a wider range of significant vibration response can sustain consistent amplitude at flow speeds that fall between the different structural mode frequencies, allowing for a higher overall efficiency of operation. However, a detailed investigation of the performance of such simple oscillating systems under loading is needed before any facts are drawn about the suitability of these systems as a basis for generating energy with proper efficiency or practicality.

5. Conclusion

In this paper, the flow over three cylinders of equal diameter arranged in-line in cross-flow with uneven spacing was numerically investigated at a Reynolds number of 200. The distance between the axes of the upstream cylinder and the most downstream cylinder was kept constant at 4.00 diameters. The flow field around the three cylinders was simulated at several locations of the middle cylinder to test the effect of uneven spacing between the cylinders on the flow patterns and flow-induced vibration response. Results show that the uneven spacing between the cylinders can trigger significant changes in the flow characteristics not observed for the case of a single cylinder or two tandem cylinders. The different arrangements of cylinders exhibit two distinctive patterns of vortex shedding, one of which causes significantly higher lift and drag and a lower Strouhal number. Besides, the change between the patterns is sensitive to the spacing between the cylinders. When the middle cylinder is located at $x = 1.60D$ or $1.80D$, flow separated on the upstream cylinder reattaches on the surface of the downstream cylinder. On the other hand, when the middle cylinder is located at all other simulated locations the separated flow does not reattach on the downstream cylinder. The occurrence of reattachment causes higher harmonics in the spectra of the lift force and leads to the formation of vortices in the gap between the middle and downstream cylinders.

To investigate the effect of these flow features on the flow-induced vibration response of the system, a numerical model is developed to simulate the vibration of the most downstream cylinder of an inline row of three cylinders in cross-flow with uneven spacing. As reduced velocity was increased, the downstream cylinder oscillates with higher amplitudes until it reaches a maximum value after which the amplitude decreases gradually. The oscillation amplitude reaches a significantly higher value than that of vortex-induced vibration of a single cylinder, indicating that the wake of the two cylinders placed upstream of the moving cylinder plays the main role in the energy exchange mechanism. At the reduced velocity that causes maximum oscillation amplitude, the flow structure around the cylinders is dominated by the motion of the downstream cylinder. Moreover, significant vibration amplitudes are maintained at high reduced velocities and the case of even spacing results in the highest displacement amplitude of $0.6D$. The high oscillation amplitudes at high reduced velocities are attributed to the varying phase between the lift force and the displacement. Investigation of the phase between lift force and cylinder displacement shows that the motion of the cylinder is significantly altered from the response of an isolated cylinder due to the effect of the wake on the moving cylinder. The wake flow introduces two opposing effects that are absent in the case of an isolated cylinder. First, the wake creates a stabilizing force that acts against the vibration cycle when the cylinder is submerged in the wake. On the contrary, the wake flow separated at the two upstream cylinders flows through the gap between the middle and the downstream cylinder. The resulting low static pressure then creates a driving force that maintains the cylinder oscillations. The driving force is more pronounced at higher reduced velocities at which the effects of the vortex-induced forces are expected to vanish. Therefore, the two contrasting mechanisms dominate the vibration response at higher reduced velocities, and high vibration amplitudes are maintained. The wider range of lock-in, and the high oscillation amplitude at high reduced velocities suggest that the arrangement of three inline cylinders can have potential use in flow energy harvesting devices.

Acknowledgment

The authors thankfully acknowledge the financial support provided by the Natural Sciences and Engineering Research Council of Canada (NSERC Discovery Grant #210313).

References

Ahn, H.T., Kallinderis, Y., 2006. Strongly coupled flow/structure interactions with a geometrically conservative ALE scheme on general hybrid meshes. J. Comput. Phys. 219 (2), 671–696.

Anagnostopoulos, P., Bearman, P., 1992. Response characteristics of a vortex-excited cylinder at low Reynolds numbers. J. Fluids Struct. 6 (1), 39–50.

Arafa, N., Mohany, A., 2015. Flow-excited acoustic resonance of multiple isolated cylinders in cross-flow. J. Press. Vessel Technol. 138 (1), 011302.

Assi, G.R.S., Bearman, P.W., Meneghini, J.R., 2010. On the wake-induced vibration of tandem circular cylinders: the vortex interaction excitation mechanism. J. Fluid Mech. 661, 365–401.

Bao, Y., Zhou, D., Tu, J., 2011. Flow interference between a stationary cylinder and an elastically mounted cylinder arranged in proximity. J. Fluids Struct. 27 (8), 1425–1446.

Barrero-Gil, A., Pindado, S., Avila, S., 2012. Extracting energy from vortex-induced vibrations: a parametric study. Appl. Math. Model. 36 (7), 3153–3160.

Bearman, P., 2011. Circular cylinder wakes and vortex-induced vibrations. J. Fluids Struct. 27 (5), 648–658.

Bernitsas, M.M., Raghavan, K., Ben-Simon, Y., Garcia, E.M., 2008. Vivace (vortex induced vibration aquatic clean energy): a new concept in generation of clean and renewable energy from fluid flow. J. Offshore Mech. Arct. Eng. 130 (4), 041101.
Borazjani, I., Sotiropoulos, F., 2009. Vortex-induced vibrations of two cylinders in tandem arrangement in the proximity–wake interference region. J. Fluid Mech. 621, 321–364.
Carmo, B.S., Meneghini, J.R., 2006. Numerical investigation of the flow around two circular cylinders in tandem. J. Fluids Struct. 22 (6), 979–988.
Carmo, B.S., Sherwin, S.J., Bearman, P.W., Willden, R.H.J., 2011. Flow-induced vibration of a circular cylinder subjected to wake interference at low reynolds number. J. Fluids Struct. 27 (4), 503–522.
Farrant, T., Tan, M., Price, W.G., 2000. A cell boundary element method applied to laminar vortex-shedding from arrays of cylinders in various arrangements. J. Fluids Struct. 14 (3), 375–402.
Govardhan, R., Williamson, C., 2006. Defining the modified Griffin plotin vortex-induced vibration: revealing the effect of Reynolds number using controlled damping. J. Fluid Mech. 561, 147–180.
Grouthier, C., Michelin, S., Bourguet, R., Modarres-Sadeghi, Y., De Langre, E., 2014. On the efficiency of energy harvesting using vortex-induced vibrations of cables. J. Fluids Struct. 49, 427–440.
Harichandan, A.B., Roy, A., 2010. Numerical investigation of low Reynolds number flow past two and three circular cylinders using unstructured grid CFR scheme. Int. J. Heat Fluid Flow 31 (2), 154–171.
Hassan, M., Mohany, A., 2013. Fluidelastic instability modeling of loosely supported multispan u-tubes in nuclear steam generators. J. Press. Vessel Technol. 135 (1), 011306.
Hover, F., Techet, A., Triantafyllou, M., 1998. Forces on oscillating uniform and tapered cylinders in cross flow. J. Fluid Mech. 363, 97–114.
Hover, F.S., Triantafyllou, M.S., 2001. Galloping response of a cylinder with upstream wake interference. J. Fluids Struct. 15 (3), 503–512.
Igarashi, T., Suzuki, K., 1984. Characteristics of the flow around three circular cylinders. Bull. JSME 27 (233), 2397–2404.
Khalak, A., Williamson, C.H.K., 1997. Fluid forces and dynamics of a hydroelastic structure with very low mass and damping. J. Fluids Struct. 11 (8), 973–982.
Lam, K., Gong, W.Q., So, R.M.C., 2008. Numerical simulation of cross-flow around four cylinders in an in-line square configuration. J. Fluids Struct. 24 (1), 34–57.
Liu, C., Zheng, X., Sung, C.H., 1998. Preconditioned multigrid methods for unsteady incompressible flows. J. Comput. Phys. 139 (1), 35–57.
Meneghini, J., Saltara, F., Siqueira, C., Ferrari, J., 2001. Numerical simulation of flow interference between two circular cylinders in tandem and side-by-side arrangements. J. Fluids Struct. 15 (2), 327–350.
Mittal, S., Kumar, V., 2001. Flow-induced oscillations of two cylinders in tandem and staggered arrangements. J. Fluids Struct. 15 (5), 717–736.
Mohany, A., 2006. Flow-Sound Interaction Mechanisms of a Single and Two Tandem Cylinders in Cross-Flow. McMaster University, (Ph.D. thesis).
Mohany, A., Janzen, V.P., Feenstra, P., King, S., 2012. Experimental and numerical characterization of flow-induced vibration of multispan u-tubes. J. Press. Vessel Technol. 134 (1), 011301.
Morse, T., Williamson, C., 2009. Prediction of vortex-induced vibration response by employing controlled motion. J. Fluid Mech. 634, 5–39.
Norberg, C., 2003. Fluctuating lift on a circular cylinder: review and new measurements. J. Fluids Struct. 17 (1), 57–96.
Papaioannou, G.V., Yue, D.K., Triantafyllou, M.S., Karniadakis, G.E., 2006. Three-dimensionality effects in flow around two tandem cylinders. J. Fluid Mech. 558, 387–413.
Parkinson, G., 1974. Mathematical models of flow-induced vibrations of bluff bodies. In: Flow-Induced Structural Vibrations.(A 75-15253 04-39), Vol. 1974. Springer-Verlag, Berlin, pp. 81–127.
Portela, G., Godoy, L.A., 2005. Wind pressures and buckling of cylindrical steel tanks with a conical roof. J. Construct. Steel Res. 61 (6), 786–807.
Sarpkaya, T., 1979. Vortex-induced oscillations: a selective review. J. Appl. Mech. 46 (2), 241–258.
Sosa, E.M., Godoy, L.A., 2005. Nonlinear dynamics of above-ground thin-walled tanks under fluctuating pressures. J. Sound Vib. 283 (1), 201–215.
Weaver, D.S., Ziada, S., Au-Yang, M.K., Chen, S.S., Paıdoussis, M.P., Pettigrew, M.J., 2000. Flow-induced vibrations in power and process plant compo-nentsprogress and prospects. J. Press. Vessel Technol. 122 (3), 339–348.
Yoshitake, Y., Sueoka, A., Yamasaki, M., Sugimura, Y., Ohishi, T., 2004. Quenching of vortex-induced vibrations of towering structure and generation of electricity using hula-hoops. J. Sound Vib. 272 (1), 21–38.
Zdravkovich, M., 1977. Review of flow interference between two circular cylinders in various arrangements. J. Fluids Eng. 99 (4), 618–633.
Zhang, J., Dalton, C., 1998. A three-dimensional simulation of a steady approach flow past a circular cylinder at low reynolds number. Internat. J. Numer. Methods Fluids 26 (9), 1003–1022.
Zhang, H.J., Zhou, Y., 2001. Effect of unequal cylinder spacing on vortex streets behind three side-by-side cylinders. Phys. Fluids 13 (12), 3675–3686.